Journal of Catalysis 272 (2010) 176–189

Contents lists available at ScienceDirect

Journal of Catalysis

journal homepage: www.elsevier.com/locate/jcat

Nature of surface sites of V_2O_5—TiO_2/SO_4^{2-} catalysts and reactivity in selective oxidation of methanol to dimethoxymethane

Hongying Zhao [a,b], Simona Bennici [a], Jianyi Shen [b], Aline Auroux [a,*]

[a] Université Lyon 1, CNRS, UMR 5256, Ircelyon, Institut de Recherches sur la Catalyse et l'environnement de Lyon, 2 Avenue Albert Einstein, F-69626 Villeurbanne, France
[b] Laboratory of Mesoscopic Chemistry, School of Chemistry and Chemical Engineering, Nanjing University, Nanjing 210093, China

ARTICLE INFO

Article history:
Received 29 October 2009
Revised 24 February 2010
Accepted 25 February 2010
Available online 3 April 2010

Keywords:
V_2O_5—TiO_2/SO_4^{2-}
TPR
Pyridine FTIR
Ammonia adsorption calorimetry
Methanol selective oxidation
Dimethoxymethane

ABSTRACT

The selective oxidation of methanol to dimethoxymethane (DMM) over sulfated vanadia–titania catalysts, prepared by co-precipitation and calcined at different temperatures, was studied in the 393–473 K interval under steady state conditions. The catalysts were characterized by X-ray diffraction (XRD), Brunauer–Emmett–Teller isotherms (BET), inductively coupled plasma optical emission spectroscopy (ICP–OES), X-ray photoelectron spectroscopy (XPS), scanning electron microscopy (SEM), transmission electron microscopy (TEM), Fourier transform infrared spectroscopy (FTIR), and Raman spectroscopy. The redox and acidic properties were examined using temperature programmed reduction (TPR), isopropanol probe reaction, ammonia adsorption calorimetry, and pyridine adsorption FTIR techniques. As evidenced by pyridine adsorption FTIR, some Brönsted acid sites transformed to Lewis sites upon removal of sulfate species by washing the samples with deionized water. A high sulfur content increased the number of Brönsted acid sites but reduced their strength. The best catalyst revealed the presence of amorphous polymeric VO_x species with terminal V=O bonds, and both redox and Brönsted acid sites, resulting from an adequate balance between the calcination temperature and the sulfate concentration. These are the key parameters for optimizing the DMM production.

1. Introduction

Dimethoxymethane (DMM) is especially interesting for industrial applications [1–4], since it is suitable as fuel additive with a high chemical stability, as solvent in the perfume industry and as reagent in organic syntheses. Industrially, DMM is produced by a two-stage process: methanol oxidation to formaldehyde on silver and ferric molybdate catalysts and dehydrative condensation of the formaldehyde with methanol in the presence of liquid and solid acids [3,4]. Thus, a one-stage heterogeneous reaction process has economical and environmental benefits in the production of DMM, where three methanol molecules are incorporated into one DMM molecule ($3CH_3OH + 1/2O_2 \rightarrow CH_2(OCH_3)_2 + 2H_2O$). It has been reported in the literature that DMM can be also synthesized by the direct oxidation of methanol on crystalline $SbRe_2O_6$ [5], Re/γ-Fe_2O_3 [6], heteropolyacids [7], RuO_x/SiO_2 [8], Cu–ZSM-5 [9], and V_2O_5/TiO_2–$Ti(SO_4)_2$ [10].

Irrespective to the catalytic system, all the studies suggest a dual mechanism involving redox and acidic sites (Brönsted in case of Keggin structures [3,11], or Lewis for Re-based catalysts [6]). Additionally, Wachs indicated that the surface Brönsted acid sites can facilitate oxidation reactions requiring the participation of dual redox-acid sites [12]. Achieving an adequate balance between the two kinds of active sites is thus a crucial prerequisite for optimal DMM production.

Furthermore, the contributions of different VO_x species to the catalytic performance have been debated for some time in previous studies [13–24]. Many researchers claim that amorphous monomeric VO_x species with terminal V=O bonds are the most active species for reactant adsorption and C–H bond breaking compared to crystalline V_2O_5 [13–15]. Grzybowska-Swierkosz [16] pointed out the necessary participation of both monomeric and polymeric species. Tatibouët [17,18] proposed that a surface site constituted by a vanadyl V=O double bond standing up and a near "oxygen vacancy" constituted by the sixth coordination of a vanadium (vanadyl down) could be the most appropriate for DMM formation. In contrast, Gervasini et al. [19] found higher catalytic activity for polymeric rather than for monomeric VO_x species in partial oxidation of o-xylene to phthalic anhydride (PA), and Van Hengstum et al. [20] reported that vanadia multilayers and/or crystallites did not affect the selective oxidation of toluene. Weckhuysen et al. [21] stated that the V–O-support bond is important in methanol oxidation, a model reaction for V_2O_5/TiO_2 catalyst. Moreover, density functional theory (DFT) has demonstrated that the oxygen atom in the V–O–Ti bond is the most reactive toward atomic hydrogen adsorption, the limiting step of the oxidation reaction, because of the high stability of terminal V=O bonds [22]. Wachs

* Corresponding author. Fax: +33 472445399.
E-mail address: aline.auroux@ircelyon.univ-lyon1.fr (A. Auroux).

0021-9517/$ - see front matter © 2010 Elsevier Inc. All rights reserved.
doi:10.1016/j.jcat.2010.02.028

and Weckhuysen [23], on the other hand, stressed the critical role of bridging oxygen in V–O-support as mentioned also by Bulushev et al. [24].

We have recently studied the reactivity of sulfated vanadia–titania catalysts prepared by various methods to selectively catalyze methanol oxidation to DMM [25]. These previous results [25,26] investigated how both the preparation method and the sulfate content impacted the DMM synthesis. In this work, the challenge lied in: (1) fixing the right amount of surface residual sulfate (with or without washing with deionized water) during the calcination step in order to tune the acidity of the coprecipitated V_2O_5—TiO_2/SO_4^{2-} catalysts and (2) developing active surface structure most appropriate for DMM synthesis during the calcination process. The VTiS samples were characterized by X-ray diffraction (XRD), Brunauer–Emmett–Teller isotherms (BET), inductively coupled plasma optical emission spectroscopy (ICP–OES), X-ray photoelectron spectroscopy (XPS), scanning electron microscopy (SEM), transmission electron microscopy (TEM), Fourier transform infrared spectroscopy (FTIR), Raman spectroscopy, ammonia adsorption calorimetry, and pyridine adsorption FTIR. This study reports, in detail, the effects of surface structure, nature, and strength of active acidic sites on the performance of the selective oxidation of methanol to DMM.

2. Experimental

2.1. Catalyst preparation

Five gram of V_2O_5—TiO_2/SO_4^{2-} catalysts were prepared by a co-precipitation method [27] with 3.2 g of $VOSO_4 \times H_2O$ and 11.5 g of $TiOSO_4 \times H_2SO_4 \times H_2O$ as precursors, and 25 mL 28 wt.% $NH_3{\cdot}H_2O$ solution as precipitant. Samples VTiS-573, VTiS-623, VTiS-673, VTiS-673, and VTiS-723 were prepared in this way, and then calcined in air for 5 h at 573, 623, 673, 723, and 773 K, respectively. Additionally, samples VTiSw50-673 and VTiSw300-673 were prepared by the same procedure of co-precipitation, washed with, respectively, 50 and 300 mL deionized water while filtering the precipitate and then calcined at given temperature of 673 K in air for 5 h.

2.2. Catalyst characterization

Elemental analysis was performed using ICP optical emission spectroscopy (ICP–OES) with an ACTIVA spectrometer from Horiba JOBIN YVON.

The surface areas and pore sizes were measured by nitrogen adsorption at 77 K on a Micromeritics 2010 apparatus after heat pretreatment under vacuum for 3 h at a temperature 100 K lower than the calcination temperature.

The X-ray diffraction (XRD) measurements were carried out on a Bruker D5005 powder diffractometer scanning from 3° to 80° (2θ) at a rate of 0.02 degree s^{-1} using a Cu Kα radiation (λ = 0.15418 nm) source. The applied voltage and current were 50 kV and 35 mA, respectively.

The X-ray photoelectron spectra were measured on a KRATOS AXIS Ultra DLD spectrometer equipped with a hemispherical electron analyzer and an Al anode (Al Kα = 1486.6 eV) powered at 150 W, a pass energy of 20 eV, and a hybrid lens mode. The detection area analyzed was 700 μm × 300 μm. Charge neutralization was required for all samples. The peaks were referenced to the C–(C, H) components of the C1s band at 284.6 eV. Shirley background subtraction and peak fitting to theoretical Gaussian–Lorentzian functions were performed using an XPS processing program (vision 2.2.6 KRATOS). The residual pressure in the spectrometer chamber was 5×10^{-9} mbar during data acquisition.

Scanning electron microscopy (SEM) was performed using a Philips 5800 SEM electron microscope. The samples were deposited onto scotch carbon and metallized by sputtering. A gold film ensures a good conductivity for the observation.

The recording of transmission electron micrographs was carried out using a JEOL 2010 equipment operating at 200 kV with a high resolution pole piece and an energy dispersive X-ray spectrometer (EDS) (Link Isis from Oxford Instruments). The samples were dispersed in ethanol using a sonicator and a drop of the suspension was dripped onto a carbon film supported on a copper grid and then ethanol was evaporated. EDS study was carried out using a probe size of 15 nm to analyze borders and centers of the particles and the small particles. Standard deviations were evaluated for atomic ratio from at least 10 analyzes.

Raman spectroscopy measurements were performed using a LabRAM HR (Jobin Yvon) spectrometer. The excitation was provided by the 514.5 nm line of an Ar^+ ion laser (Spectra physics) employing a laser power of 100 μW. The laser beam was focused through microscope objective lenses (100×) down to a 1-μm spot on the sample.

H_2-TPR measurements were performed using a TPD/R/O-1100 instrument (ThermoFisher). Prior to the TPR run, the fresh sample was treated in a stream of O_2/He (0.998% v/v, flowing at 20 mL min^{-1}), ramping the temperature at 10 K min^{-1} from RT to a temperature 100 K lower than the calcination temperature and maintaining it for 60 min, and then cooled to 313 K. The TPR measurement was carried out using H_2/Ar (4.98% v/v) as reducing gas mixture, flowing at 20 mL min^{-1}. The heating rate was 10 K min^{-1} from 313 K to 1073 K. The H_2 consumption was detected by a thermal conductivity detector (TCD). The sample size used was adjusted in order to have around 69 μmol of V_2O_5 independently of the vanadia loading of the sample. This allowed us to maintain a *K* value of 100 s. (The characteristic number, *K*, can be used to facilitate the selection of appropriate operating parameters; a fixed *K* value between 60 and 140 s guarantees optimal conditions to obtain good TPR profiles [28,29].) The TPR peak areas were calibrated with given H_2/Ar (4.98% v/v) mixture injections.

The skeletal FTIR and pyridine adsorption FTIR spectra were recorded at room temperature with a Bruker Vector 22 FTIR spectrophotometer (DTGS detector) operating in the 4000–400 cm^{-1} range, with a resolution of 2 cm^{-1} and 100 acquisition scans. In each skeletal FTIR experiment, 2 mg of sample was mixed with 198 mg of KBr. In each pyridine adsorption FTIR measurement, the self-supporting wafer (10–30 mg, 18 mm diameter) was first activated in situ at a temperature 100 K lower than the calcination temperature in oxygen flow for 14 h, then evacuated at the same temperature for 2 h and then exposed to pyridine (air liquid, 99.8%, vapor pressure 3.3 kPa) at room temperature for 5 min. The desorption was carried out by evacuation for 30 min each at room temperature, 373 K, 473 K, and 573 K, respectively. The spectra were recorded at room temperature after adsorption and desorption at each temperature.

The microcalorimetric studies of ammonia adsorption were performed at 423 K in a heat flow calorimeter (C80 from Setaram) linked to a conventional volumetric apparatus equipped with a Barocel capacitance manometer for pressure measurements. Ammonia used for measurements (air liquid, purity > 99.9%) was purified by successive freeze–pump–thaw cycles. About 100 mg of sample was pretreated in a quartz cell under evacuation overnight at a temperature 100 K lower than the calcination temperature. The differential heats of adsorption were measured as a function of coverage by repeatedly introducing small doses of ammonia gas onto the catalyst until an equilibrium pressure of about 66 Pa was reached. The sample was then outgassed for 30 min at the same temperature, and a second adsorption was performed at 423 K until an equilibrium pressure of about 27 Pa was

attained in order to calculate the irreversibly chemisorbed amount of ammonia at this pressure.

2.3. Catalytic reactions

The reaction of isopropanol conversion was used to characterize the surface acidity. This probe reaction was carried out in a fixed-bed glass tube reactor. About 100 mg of sample was loaded for each reaction. Isopropanol was introduced onto the catalyst by bubbling air through a glass saturator filled with isopropanol maintained at 295 K. Isopropanol and reaction products were analyzed by an online gas chromatograph (GC), using a polyethylene glycol (PEG) 20 M packed column connected to a Flame Ionization Detector (FID). Prior to the test, each catalyst was pretreated by heating in air at the same temperature as that used for calcination for 1 h and then cooled in the air flow to the reaction temperature.

The oxidation of methanol was carried out in a fixed-bed microreactor made of glass with an inner diameter of 6 mm. The methanol was introduced into the reaction zone by bubbling O_2/N_2 (1/5) through a glass saturator filled with methanol (99.9%) maintained at 278 K. In each test, 0.2 g of catalyst was loaded, and the gas hourly space velocity (GHSV) was 11,400 mL g^{-1} h^{-1}. The feed composition was maintained as methanol:O_2:N_2 = 1:3:15 (v/v). The tail gas out of the reactor was analyzed by an online GC equipped with an FID detector and a thermal conductivity detector (TCD). The column used was PORAPAK N for the separation of methanol, DMM, and other organic compounds. The gas lines were kept at 373 K to prevent condensation of the reactant and products. The reaction was carried out at atmospheric pressure. Prior to the test, the samples were pretreated in the same way as for the isopropanol conversion reaction.

3. Results and discussion

3.1. Surface structures

The XRD patterns of the VTiS catalysts are presented in Fig. 1. It can be seen from the figure that typical diffraction peaks characteristic of anatase TiO_2 were observed for all VTiS catalysts. In particular, the VTiS-573 and VTiS-623 samples exhibited broader diffraction patterns indicating the much more amorphous nature of their TiO_2 species. The intensity of the peaks due to anatase TiO_2 increased with increasing calcination temperature, indicating agglomeration of TiO_2 particles. Crystalline V_2O_5 was detected only for samples calcined at 723 and 773 K, suggesting that vanadium oxide was present in a highly dispersed manner at low calcination temperature. In addition, the average sizes of V_2O_5 and TiO_2 particles as determined by the Debye–Scherrer formula from the XRD data are presented in Table 1. Upon increasing the calcination temperature, the titania particle size increased from 1 nm (VTiS-573) to 4 nm (VTiS-673), and then increased to 15 nm (VTiS-723) and 18 nm (VTiS-773). The average sizes of crystalline V_2O_5 were found to be 18 nm for VTiS-723 and 22 nm for VTiS-773, indicating the aggregation of particles.

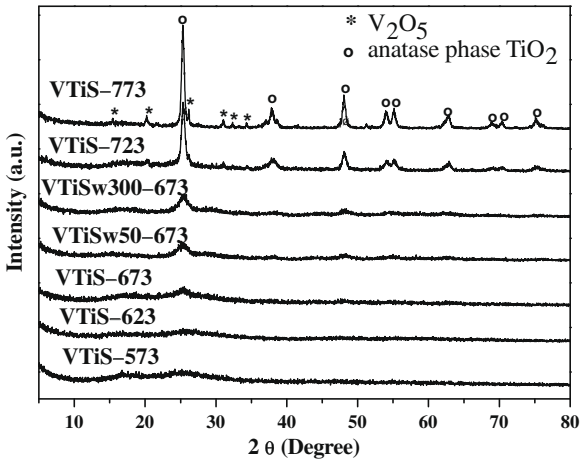

Fig. 1. X-ray diffraction (XRD) patterns of VTiS and VTiSw catalysts.

The BET surface area, porosity data, bulk (ICP) and surface (XPS) analysis for all studied VTiS catalysts are given in Table 1. The surface areas continuously decreased from 402 to 57 m^2 g^{-1} along with the average pore size which increased from 8.1 to 31.7 nm with increasing calcination temperature. The structure of VTiS catalysts did not change after washing with deionized water. The concentration of sulfur and nitrogen decreased drastically with increasing calcination temperature (especially for $T_{cal.} \geqslant 723$ K) and/or washing with deionized water, suggesting that the sulfur species were not tightly anchored to the support surface.

Table 2 lists the binding energies of V2$p_{3/2}$, O1s, S2$p_{1/2}$, and N1s and relative components from the decomposition of the O1s and V2$p_{3/2}$ lines. The reference V2$p_{3/2}$ peak positions for V_2O_5 and V_2O_4 are around 517.5 and 516.4 eV, respectively [30,31]. The full oxidation state (+5) of vanadia was predominant at catalyst surface. The formation of 20–30% V^{4+} species may be due to the exposure of the catalysts to X-radiation under ultra-high vacuum (UHV) operating conditions.

As seen in Table 2, the O1s spectra were identical and can be divided into three peaks respectively at ~530.4 eV (lattice oxygen of $TiO_2 + V_2O_5$ oxides contribution), ~513.2 eV (–OH contribution), and ~532.0 eV (sulfate oxygen contribution). The trend of sulfate oxygen content varied with the concentration of sulfur as shown by ICP and XPS, suggesting that the sulfur compound exists in the SO_4^{2-} form. The N1s line at binding energy around 400.0–401.2 eV may be due to an uncompleted decomposition at 553 K of ammonium salts formed during the preparation method [31]. In addition, the S2$p_{1/2}$ line at the binding energy of about 169.0 eV is typical of sulfur in S^{6+} oxidation state, such as in Na_2SO_4 or $Fe_2(SO_4)_3$ [32,33].

The surface structure of vanadia and titania species present on the VTiS catalysts was examined by Raman spectra, from 1500 to 200 cm^{-1}, as shown in Fig. 2. No Raman band was observed for VTiS-573 and VTiS-623 samples, possibly due to the presence of highly amorphous VO_x species on the surface. Since the BET surface area of catalysts decreased with increasing calcination temperature, polymeric vanadate species could have developed on the catalyst surface. The pronounced Raman bands at 1034 cm^{-1} assigned to terminal V=O bond and at 943 cm^{-1} due to V–O–V linkage for polymeric vanadate species were detected for samples calcined at 673 K [34–36]. As reported in the literature [37], the presence of surface sulfate species slightly perturbs the molecular structure of the surface vanadia species by broadening the 1034 cm^{-1} Raman band. In addition, there is a possibility of cleavage of the V–O–V bridge at high total sulfates amount, favoring the formation of $VO_2(SO_4)_2^{3-}$ species, which are more stable and having higher molecular symmetry [38]. In Fig. 2, the intensity of the band at 943 cm^{-1} decreased after washing the samples with deionized water thus indicating an overlapping of the SO_4^{2-} symmetrical stretch band in $VO_2(SO_4)_2^{3-}$ with the V–O–V band at 943 cm^{-1} [39]. Furthermore, crystalline V_2O_5 was formed when the calcination temperature reached 723 K (V_2O_5 has Raman bands around 996, 703, 530, 483, 406, 306, and 285 cm^{-1}) [40,41]. The bands at 642, 516, and 404 cm^{-1} are corresponding to Ti–O groups [42].

FTIR compared with Raman spectroscopy provides complementary information about the nature of surface metal oxide species. The skeletal FTIR spectra of VTiS samples are reported in Fig. 3a,

Table 1
Chemical analysis, X-ray photoelectron spectroscopy analysis, surface area and porosity data of the samples and calculated average size of V_2O_5 and TiO_2 particles.

Sample	C.A. (wt.%)			XPS (wt.%)				S_{BET} (m^2/g)	Average pore diameter (nm)	Pore volume (ml g^{-1})	Particle average size (nm)	
	V	Ti	S	V	Ti	S	N				V_2O_5	TiO_2
VTiS-573	10.4	33.9	3.2	11.2	31.6	5.0	2.9	402	8.1	0.8	–	1
VTiS-623	10.9	34.7	4.0	11.3	32.6	4.7	2.2	368	9.4	0.9	–	2
VTiS-673	12.6	41.0	2.6	12.3	34.7	3.7	1.7	287	11.3	0.9	–	4
VTiSw50-673	13.1	39.9	0.8	15.3	36.5	1.1	–	290	10.7	0.9	–	5
VTiSw300-673	12.6	41.6	<0.1	15.7	37.6	–	–	289	13.3	1.1	–	6
VTiS-723	12.8	43.0	0.7	14.8	37.7	2.5	1.0	100	24.1	0.6	18	15
VTiS-773	13.4	44.4	<0.1	12.2	41.0	–	0.6	57	31.7	0.5	22	18

Table 2
Binding energies of surface species and concentration (in atomic %) of different oxygen ($TiO_2 + V_2O_5$, –OH and SO_4^{2-}) and vanadia species present on the surface of the VTiS catalysts.

Sample	Binding energy (eV)						
	V2$p_{3/2}$		O1s			S2$p_{1/2}$	N1s
	V_2O_4	V_2O_5	$TiO_2 + V_2O_5$	–OH	SO_4^{2-}		
VTiS-573	516.6(25%)	517.6(75%)	530.4(54%)	531.1(7%)	532.0(39%)	168.9	401.0
VTiS-623	516.5(22%)	517.6(78%)	530.4(54%)	531.2(12%)	532.1(34%)	169.0	401.2
VTiS-673	516.4(22%)	517.7(78%)	530.4(63%)	531.1(7%)	532.0(30%)	169.9	400.2
VTiSw50-673	516.4(28%)	517.5(72%)	530.3(79%)	531.4(12%)	532.2(9%)	168.8	–
VTiSw300-673	516.2(30%)	517.4(70%)	530.2(88%)	531.4(12%)	–	–	–
VTiS-723	516.5(18%)	517.7(82%)	530.3(65%)	531.0(20%)	532.1(14%)	168.9	400.3
VTiS-773	516.2(19%)	517.4(81%)	530.1(88%)	530.9(12%)	–	–	400.1

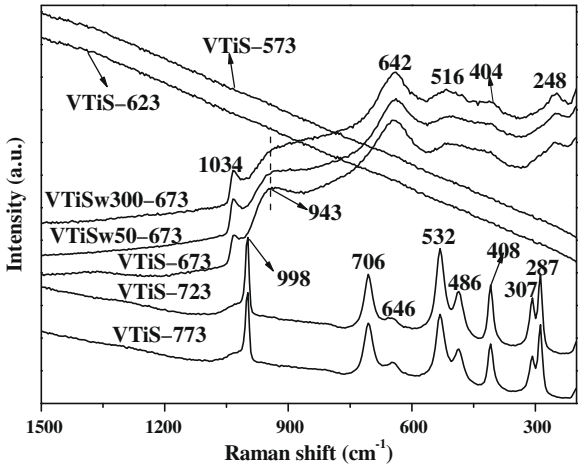

Fig. 2. Raman spectra of VTiS and VTiSw catalysts.

and the spectrum of pure TiO_2 (Millennium* G5, uncalcined) containing 0.17 wt.% sulfur (analyzed by ICP) is given for comparison. The two bands at 3430 and 1628 cm^{-1} attributed to hydrogen bonded O–H groups and H–O–H groups, respectively, were observed for all samples, and confirmed by XPS analysis of the O1s band (see Table 2). It suggests that the samples contained a certain number of surface hydroxyl groups, although some samples were calcined as high as 773 K. For pure TiO_2 as reference, other four bands at 1402, 1126, and 1051 cm^{-1} were observed; the first band was assigned to the asymmetric stretching mode of SO_2 in covalent sulfate species ($(TiO)_2SO_2$) [43,44], while the latter two originated from surface vibrations incorporating water molecules causing deformation of the surface TiO_6 octahedra surrounding surface Ti atoms [45]. For VTiS catalysts, bands at 1402, 1135, and 1050 cm^{-1} are depicted in addition to a small band at 1201 cm^{-1}. It appears that the addition of vanadia modified the spectrum obtained for TiO_2 in doing some changes such as shifting the bands at 1126, 1051 cm^{-1}, respectively, into 1135, 1060 cm^{-1} and the appearance of a new band at 1201 cm^{-1}. This indeed suggests that a strong interaction could occur between vanadia, titania, and sulfate species. The weak band at 1201 cm^{-1} could be ascribed to the asymmetric stretching mode of S–O linkages in the form of $(VO)_2SO_2$ [44], due to the migration of vanadium ions into the TiO_2–SO_4^{2-} vacant positions, but more extensive tests are required to prove this definitively. The intensities of the 1201 and 1402 cm^{-1} bands of VTiS catalysts decreased even vanished with increasing calcination temperature, as shown in Fig. 3a, which is in harmony with the XPS and ICP investigations for sulfate concentration. Inversely, a sharp band at 1030 cm^{-1} assigned to the V=O stretching vibration mode of crystalline V_2O_5 appeared when the calcination temperature reached 723 K. A large band in the range of 500–900 cm^{-1} centered at 647 cm^{-1} is probably characteristic of Ti–O–Ti anatase structure or due to vanadate species in the interlayer spaces.

Fig. 3b displays the spectra of washed VTiSw catalysts. The intensity of the band at 1201 cm^{-1} ascribed above to sulfated species decreased by washing with water, accordingly to the foregoing ICP and XPS results that the sulfate concentration drastically decreased by washing. In addition, the intensity of the band at 1135 cm^{-1} characteristic of incorporated water molecules interacting with Ti^{4+} also decreased, thus indicating that the sulfate species may impact this weak interaction by polarizing the H–O–H bond.

Fig. 3c displays the spectra of the same catalysts before (fresh VTiS–$T_{cal.}$) and after (used VTiS–$T_{cal.}$) catalytic test of methanol conversion. It can be seen that the intensity of the bands assigned to surface hydroxyl groups (at ~3430, 1628, 1135 and 1060 cm^{-1}) and the bands corresponding to sulfate species (at ~1402 and 1201 cm^{-1}) decreased after the catalytic reaction. However, the band at 1030 cm^{-1} due to V=O bonds of crystalline V_2O_5 remained the same in terms of position and intensity before and after catalytic reaction. This reflected to some extent that appropriate surface groups ($-OH + SO_4^{2-}$) may be the active sites of the catalysts, but superfluous ones can have an adverse effect on catalytic activity.

The morphology of the VTiS catalysts has been examined by electron microscopy as shown in Figs. 4 and 5. The image of

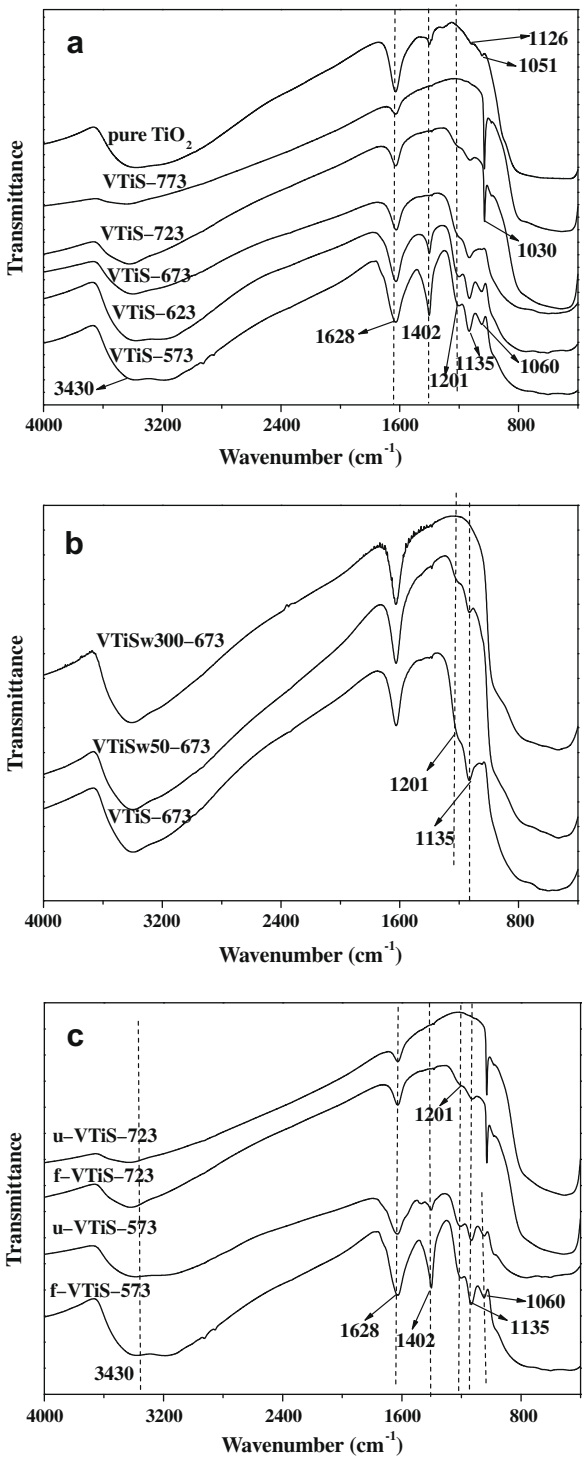

Fig. 3. FTIR skeletal spectra of: (a) VTiS catalysts and (b) VTiSw catalysts (c) catalysts before (fresh VTiS–$T_{cal.}$) and after (used VTiS–$T_{cal.}$) catalytic test of methanol conversion.

VTiS-573, presented in Fig. 4a, shows cauliflower-shaped species, which are constituted of small particles. Increasing the calcination temperature would result progressively in a loss of structure, i.e., decreased BET surface area and pore volume and increased pore diameter. Thus, for sample calcined at 623 K, the appearance of plate-shaped species was observed due to the aggregation of sample particles (shown in Fig. 4b), implying lower porosity. This phenomenon is more evident at the higher calcination temperature of 673 K as shown in Fig. 4c. Upon increasing the calcination temperature from 673 K to 723 K, an apparent change in morphology was observed for sample VTiS-723 (Fig. 4d) with the formation of needle-like crystalline particles on the surface. Moreover, the aggregation of needle-like particles was observed for sample VTiS-773 when raising the calcination temperature up to 773 K (Fig. 5a). As example, the morphology of VTiS-773 is shown in Fig. 5, which gives mainly morphological information with magnification varying from 1000× (Fig. 5a) to 20,000× (Fig. 5c). Besides the already known cauliflower-shaped species, the existence of needle-like crystals was detected on the surface of cauliflower-shaped particles (Fig. 5b and c) [46]. The morphology of VTiS-773 was deeply analyzed by TEM, and its composition (EDS) is also given, as shown in Fig. 6. The white needles are composed mainly of vanadia, while the darker part composed of numerous platelet-like particles is constituted of titania, indicating that needle-like crystals were growing away from the titania support surface. In addition, the TiO_2 particles present on samples VTiS-723 and VTiS-773 displayed irregular platelet-like shapes with dimensions of approximately 22 nm × 16 nm (obtained by TEM), which is consistent with the calculated particle size of TiO_2 shown in Table 1. However, the dimension of the needle-like vanadia crystallites was difficult to estimate from TEM analysis.

3.2. Surface acidity

3.2.1. Ammonia adsorption calorimetry study

Surface acidity, determined by ammonia adsorption calorimetry [47], expressed in terms of initial adsorption heat (denoted by Q_{init}) and amounts of ammonia adsorbed under an equilibrium pressure of 27 Pa, is shown in Table 3. The differential heats of adsorption vs. ammonia uptake (expressed in μmol NH_3 $m^{-2}_{catalyst}$) on VTiS and VTiSw catalysts are presented in Fig. 7a and b, respectively. The acid site strength distributions of the same catalysts, providing the number of sites of a given strength, are displayed in Fig. 8.

As can be seen in Fig. 7a, samples VTiS-573 and VTiS-623 exhibited quite strong acidic properties since the initial heats were 185 and 241 kJ mol^{-1}, respectively. Considering the experimental error involved in measuring the initial heat of adsorption, the initial heat slightly decreased, except for sample VTiS-673, with increasing calcination temperature. The surfaces of these catalysts appeared as heterogeneous with a continuous decrease of the energy as a function of the ammonia coverage. A particular behavior was however observed for sample VTiS-673 with low initial heats, which increased with coverage. This behavior was already reported in a previous paper [25] for sulfated vanadia–titania catalysts prepared by sol–gel and chemical grinding. This strange phenomenon was explained by a combination of both an endothermic effect such as NH_3 dissociation [48] or formation of ammonium sulfite [49] and the exothermic adsorption. However, such an effect with a lower extent was only observed for sample VTiS-673 and not for VTiS-573 and VTiS-623 samples, which contained higher sulfate concentrations. This observation indicates that the appearance of low initial heat might be related to the nature and strength of sulfate-carrier interactions created by appropriate calcination temperature.

In order to determine how the sulfate concentration impacts the surface acidity on VTiS catalysts, the acidity behavior of VTiS-673 catalyst with 2.58 wt.% sulfur (ICP) was compared with VTiSw catalysts washed with different amounts of deionized water before calcination at the same temperature of 673 K (Fig. 7b). The removal of sulfate from surface eliminated the low initial heat of adsorption previously obtained for the VTiS-673 catalyst at low ammonia uptake (<0.13 μmol m^{-2}). Beyond this value, the profiles of the three curves are similar, characteristic of vanadia–titania catalysts. This observation indicates that a high concentration of sulfur species

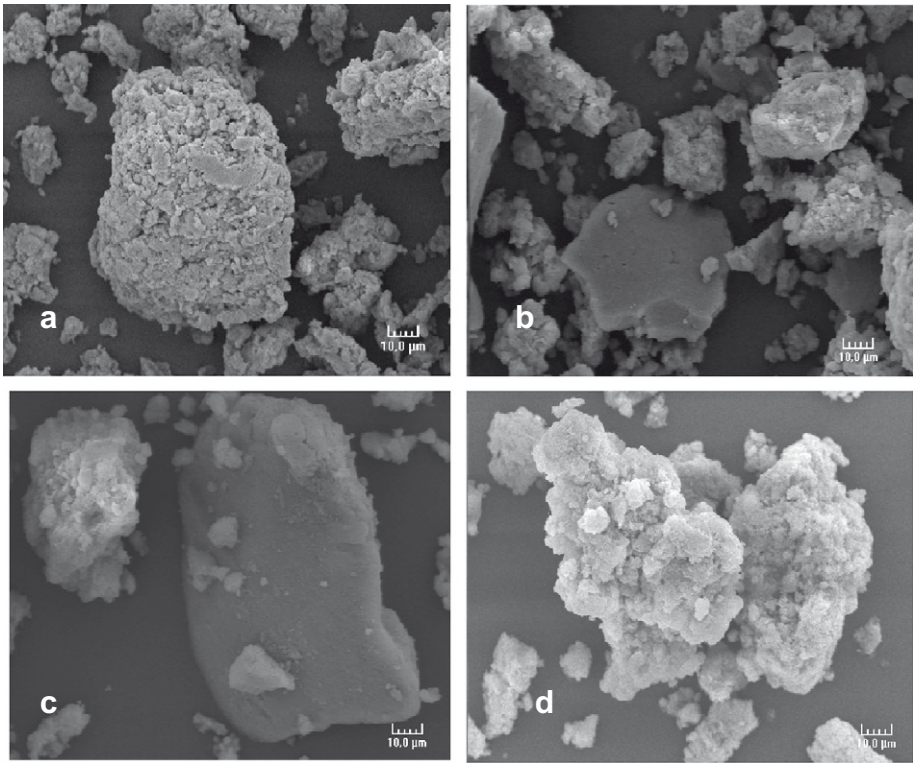

Fig. 4. SEM images of: (a) VTiS-573, (b) VTiS-623, (c) VTiS-673, and (d) VTiS-723 catalysts at the magnification of 1000×.

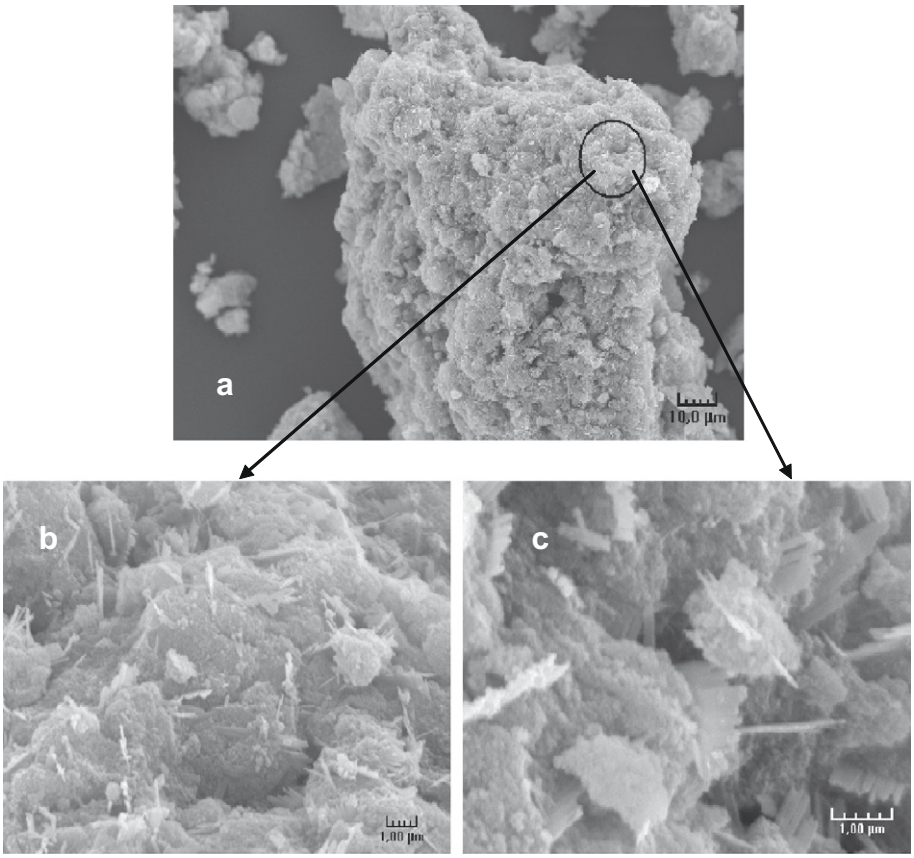

Fig. 5. SEM images of VTiS-773 catalysts at different magnifications: (a) 1000×, (b) 10,000× and (c) 20,000×.

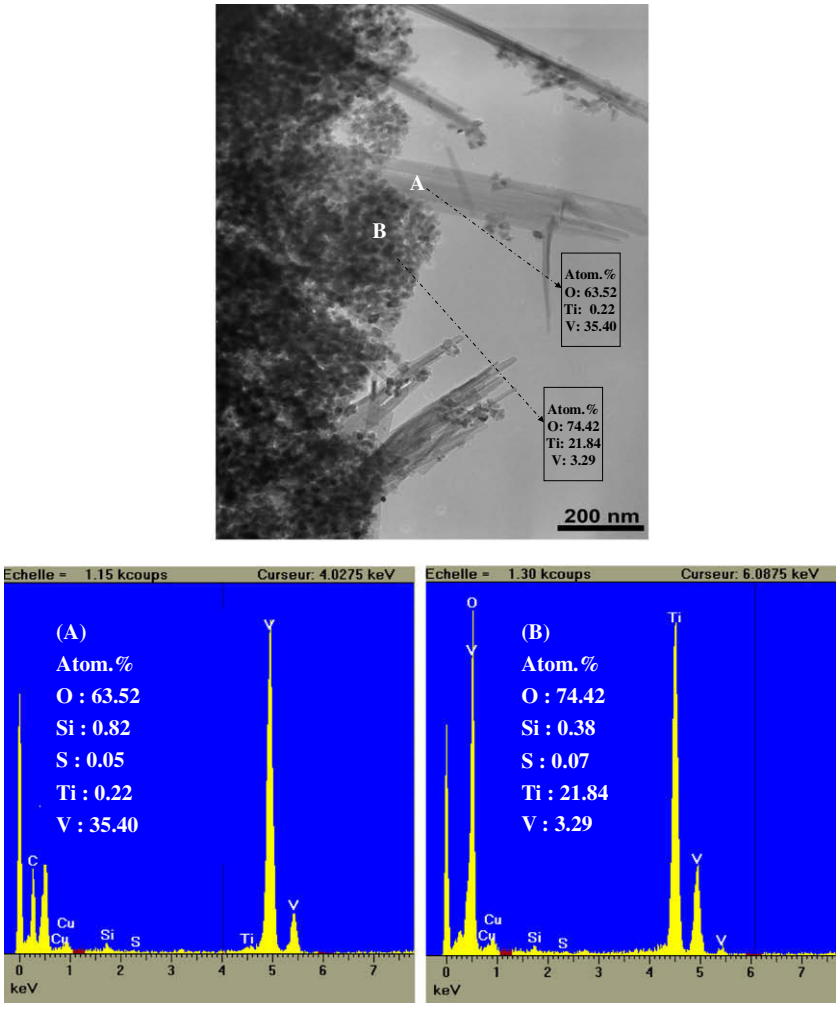

Fig. 6. TEM image and EDS spectra of VTiS-773 catalyst at the magnification of 50,000×.

Table 3
Calorimetric data for ammonia adsorption at 423 K on VTiS and VTiSw catalysts.

Sample	V_{total}[a] (μmol g^{-1})	V_{total}[a] (μmol m^{-2})	V_{irrev}[b] (μmol g^{-1})	V_{irrev}[b] (μmol m^{-2})	Q_{init}[c] (kJ mol^{-1})
VTiS-573	578	1.4	264	0.7	185
VTiS-623	591	1.6	358	1.0	241
VTiS-673	608	2.1	374	1.3	112
VTiSw50-673	568	2.0	319	1.1	253
VTiSw300-673	551	1.9	275	1.0	198
VTiS-723	268	2.7	131	1.3	190
VTiS-773	163	2.9	69	1.2	135

[a] Amount of NH_3 adsorbed under an equilibrium pressure of 27 Pa.
[b] Amount of irreversible chemisorbed NH_3.
[c] Heat evolved from the first ammonia dose.

could significantly modify only the relatively strong acidity of VTi catalysts.

In Table 3, the amount of irreversibly adsorbed ammonia, corresponding to chemisorption, decreased upon increasing calcination temperature, while the density of strong acid sites became similar when V_{irrev} is expressed per unit surface area, which confirms the role played by surface area in determining the acidity.

Fig. 8 displays the acid site strength distribution of the studied catalysts, calculated from the differential heats of NH_3 adsorption. In order to correlate with the pyridine adsorption FTIR data, this figure gives the number of acidic sites expressed in μmol g^{-1} instead of μmol m^{-2}. The strong acid sites with $Q_{diff} > 120$ kJ mol^{-1} can be ascribed to strong Lewis acid sites, while medium acid sites with $90 < Q_{diff} < 120$ kJ mol^{-1} could be assigned to Brönsted acid sites. The weak sites with $55 < Q_{diff} < 90$ kJ mol^{-1} can be considered as the physisorption sites on the catalysts surface [50]. The strange phenomenon of low initial heats of adsorption at low ammonia coverage for sample VTiS-673 makes it very difficult to calculate the number of strong acid sites ($Q_{diff} > 120$ kJ mol^{-1}). However, from the calculation on VTiSw catalysts, we can suggest that the number of strong acid sites increases with increasing calcination temperature ($T_{cal.}$) up to 673 K, then decreases when $T_{cal.} \geqslant 723$ K. In addition, the total number of acid sites including strong, medium, and weak acid sites for VTiS-723 and VTiS-773 obviously de-

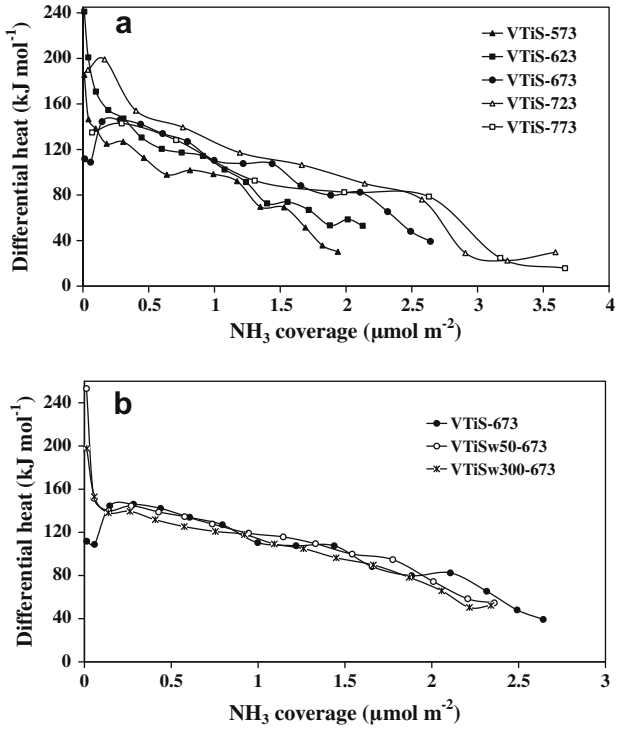

Fig. 7. Differential heats of ammonia adsorption vs. the adsorbed amount on (a) VTiS catalysts and (b) VTiSw washed catalysts.

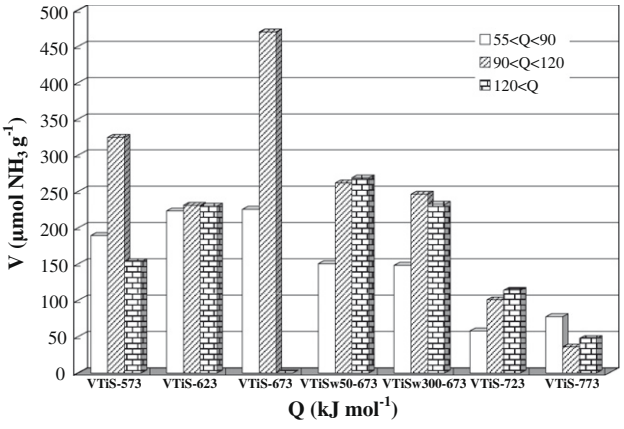

Fig. 8. Acid strength spectra of VTiS and VTiSw catalysts.

creased compared to other samples, possibly due to lower surface areas. The number of medium strength acid sites with $90 < Q_{diff} < 120$ kJ mol^{-1}, considered to be the active Brönsted acid sites as confirmed by pyridine FTIR measurements (see below), was found to be the highest for sample VTiS-673.

3.2.2. Pyridine adsorption FTIR study

Chemisorption of pyridine followed by FTIR spectroscopy is useful to probe the presence and nature of surface acid sites on catalysts [51–53]. Fig. 9 presents the FTIR spectra of pyridine adsorption on VTiS and VTiSw catalysts after desorption at 373 K for 30 min. All the spectra reported in Fig. 9 were obtained by subtracting the spectrum of the fresh catalyst (without pyridine adsorption at room temperature) from those obtained after pyridine adsorption. The bands at 1639 and 1537 cm^{-1} were attributed to Brönsted acid sites (Bpy), while the bands at 1609 and

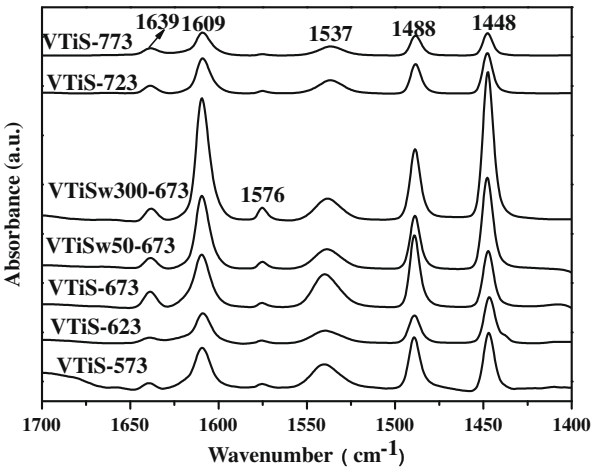

Fig. 9. FTIR spectra for pyridine adsorption and desorption at 373 K on VTiS and VTiSw catalysts.

1448 cm^{-1} corresponded to Lewis acid sites (Lpy). The bands around 1490 and 1576 cm^{-1} were associated to both Brönsted and Lewis acid sites [53].

Two Brönsted and Lewis acid site bands around ~1537 and 1448 cm^{-1}, respectively, can be used to compare the acidity by band-separation techniques of spectra [25,53,54]. The relative concentration of Brönsted and Lewis acid sites was deduced from measuring the area under the BPy and LPy peaks. In this work, the quantitative comparison of Brönsted and Lewis acid sites' population was estimated by using the same analysis method.

Fig. 10a and b show the integrated intensities of the BPy (1537 cm^{-1}) and LPy (1448 cm^{-1}) bands for VTiS and VTiSw cata-

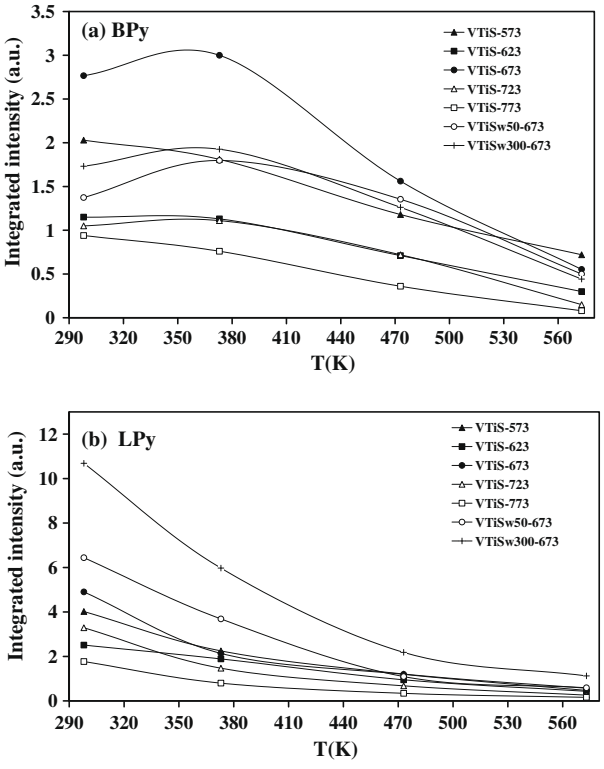

Fig. 10. Integrated intensities relative to (a) BPy band (1537 cm^{-1}) and (b) LPy band (1448 cm^{-1}) vs. evacuation temperature, after pyridine adsorption at room temperature.

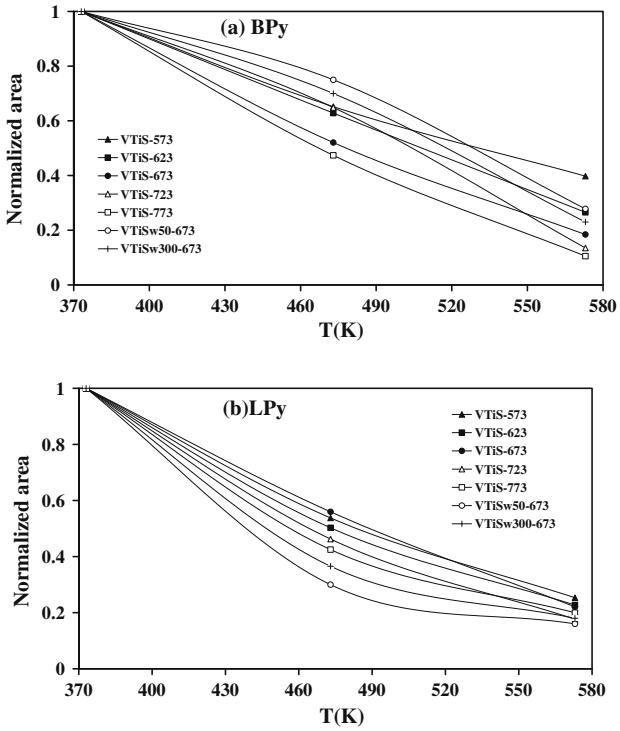

Fig. 11. Normalized area (see text) relative to: (a) BPy band (1537 cm^{-1}) and (b) LPy band (1448 cm^{-1}) vs. evacuation temperature, after pyridine adsorption at room temperature.

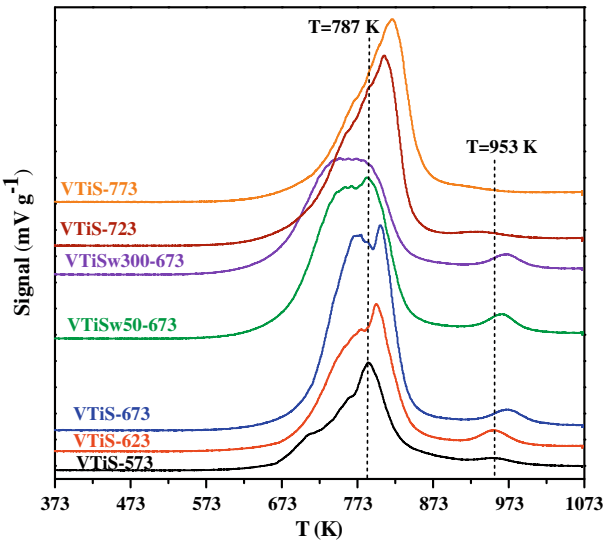

Fig. 13. TPR profiles of the VTiS and VTiSw catalysts (VTiS-573: black; VTiS-623: red; VTiS-673: blue; VTiSw50-673: olive green; VTiSw300-673: violet; VTiS-723: purple; VTiS-773: orange). (For interpretation of the references to colors in this figure caption, the reader should refer to the web version of the article.)

lysts. Assuming the possibility of physical re-adsorption with increasing evacuation temperature, it was reasonable to compare the acid sites populations at an evacuation temperature higher than 400 K. The concentration of Brönsted acid sites was found to be higher for sample VTiS-673, which was also revealed by ammonia adsorption calorimetry as shown in Fig. 8. Moreover, the number of Brönsted acid sites varied in the order VTiS-673 > VTiSw50-673 ≈ VTiSw300-673 > VTiS-573 > VTiS-623 ≈ VTiS-723 > VTiS-773, which is in agreement (except for sample VTiS-573) with the trend of the number of medium strength acid sites ($90 < Q_{diff} < 120$ kJ mol^{-1}) presented in Fig. 8. This tendency reveals that the polymeric VO_x species present on titania favor the formation of Brönsted acid sites more than crystalline vanadia species growing away from the titania support. Comparing the intensities of these two bands for VTiS-673 and the corresponding washed samples (VTiSw50-673 and VTiSw300-673), it can be seen that the concentration of Brönsted acid sites decreased with the sulfur loss. In addition, the concentration of Lewis sites increased while the Brönsted acid sites population decreased after washing with deionized water. Indeed, the presence of Brönsted acidity on VTiS catalysts can be attributed to two factors: (a) residual SO_4^{2-} and (b) the presence of defect sites [55]. Sulfate ions impact Brönsted acid character either by polarization of the O–H bond due to inductive effects or by formation of weak O–H bonds by interaction with adsorbed water. Furthermore, based on the existing theories [55,56] of predicting Brönsted acidity in the vanadia–titania system, a hypothetical reaction for transformation of Brönsted acidity to Lewis acidity induced by washing can be proposed in Fig. 12. In this reaction, two types of Brönsted acidity are respectively associated with: (type A) polarized water molecules attracted to exposed Ti^{4+} ions, as they fill the coordination sphere, and (type B) the creation of bridging hydroxyls formed between the surface vanadia and titania species. The Lewis acidity is related to unsaturated Ti ions exposed at the surface. According to this reaction, it can be seen that a progressive dehydration of acidic solid may occur due to the sulfate species loss during washing, with consequent transformation of Brönsted into Lewis acid sites. The phenomenon that the intensity of skeletal FTIR spectra bands at 1135 and 1201 cm^{-1}

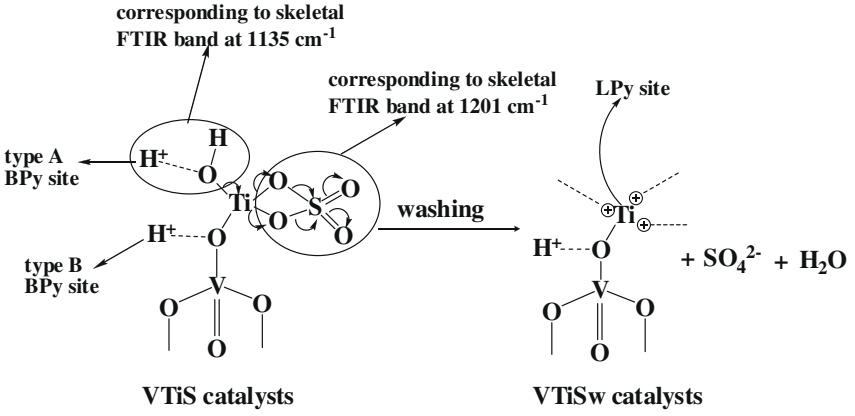

Fig. 12. Hypothetical reaction for the transformation of Brönsted acid sites to Lewis sites.

decreased after washing with water, as shown in Fig. 3b, supported this hypothetical reaction.

Meanwhile, a semiquantitative study of the strength of acid sites was carried out. To evaluate this parameter, normalized area at temperature T was defined as the ratio of the (Brönsted or Lewis) adsorption band area, measured after pyridine adsorption followed by evacuation at temperature T, to the area of the same band, measured after adsorption followed by evacuation of the probe at 373 K [57]. This quantity, calculated for Brönsted (1537 cm^{-1}) and Lewis (1448 cm^{-1}) sites adsorption bands, has been plotted as a function of evacuation temperature, as shown in Fig. 11a and b, respectively. Note that in Fig. 11a, samples VTiSw50-673 and VTiSw300-673 exhibited stronger Brönsted acidity than sample VTiS-673, which possessed the highest concentration of Brönsted acidity of unwashed samples, indicating that a high content of sulfur favored the formation of weak Brönsted acid sites (type A in Fig. 12) and thus to some extent inhibited the creation of strong acid sites. In addition, for Lewis acidity, sample VTiSw300-673 showed the highest concentration of Lewis acid sites but the lowest strength as observed in Figs. 10b and 11b, indicating that removal of sulfate from the surface weakened the Lewis acidity [58].

3.3. Reducibility of surface vanadia species by hydrogen

TPR is frequently used to study the redox properties. It is possible to correlate the redox properties with the presence of different VO_x surface species [59,60]. Normalized TPR profiles of the VTiS and VTiSw catalysts are shown in Fig. 13. The maximum reduction temperatures (T_{m1} and T_{m2}), the hydrogen consumption (expressed in μmol g^{-1}), and the theoretical surface vanadium loading (V nm^{-2}) are presented in Table 4.

The calculated surface vanadium loading, to some extent, indicates the nature of VO_x species. At low loadings (up to 2–3 V nm^{-2}), strongly bound monomeric VO_x groups with three V–O bonds to the support and a terminal partly hydrated V=O bond are formed at ambient conditions [61]. At V coverage greater than about 3 V nm^{-2}, some V–O-support bridges rearrange themselves into V–O–V bridges [16,19,62] increasing the degree of polymerization. These still-amorphous vanadia species turn into crystalline ones when the V coverage exceeds about 8 V nm^{-2} [16].

The TPR profiles of the samples with low surface vanadium loading, around 3–5 V nm^{-2}, exhibited two distinct peaks, indicating the presence of several types of oxygen-containing vanadium species on the titania surface. One peak is in the low-temperature region (T_{m1} < 873 K), while the other peak is in the high-temperature region (873 K < T_{m2} < 1023 K). Since the temperature programmed reduction treatment up to 1073 K may induce structural changes in the catalysts, the high temperature peak at 873–1023 K is most probably due to bulk V_2O_5 issued from monomeric or polymeric VO_x species at such high temperature [26]. Therefore, only the low temperature reduction peaks (T_{m1} < 873 K) were used to estimate the different surface VO_x species possibly present on the catalyst. For sample, VTiS-573, a peak (T_{m1} = 787 K) with two small shoulders at lower temperatures (708 and 763 K) was observed. With increasing calcination temperature, the surface vanadium coverage increased and the maximum temperature of the reduction peak (T_{m1}) shifted to higher values, indicating that the amount of surface vanadia species increased and more polymeric vanadia species might be formed. For example, the TPR profile of sample VTiS-623 showed a main peak centered at 798 K with a shoulder at 777 K, while the TPR profile of sample VTiS-673 exhibited a peak with two maxima at 775 and 805 K. The intensity of the left-hand shoulder maximizing around 763–775 K increased obviously by rising the calcination temperature, most possibly due to an increased amount of reducible VO_x species, i.e., an increased percentage of V^{5+} oxidation state and/or an increased amount of vanadium centers in strong interaction with the support. Additionally, from the comparison of the TPR profiles of catalysts VTiS-673 and VTiSw-673 (washed), it is noteworthy to see that the intensity of the main TPR peak decreased and that the maximum temperature of this peak slightly shifted to lower values after washing with water. These results reveal that the addition of sulfate might slightly inhibit the reduction of vanadia species and the main TPR peak, presenting either a shoulder or two maxima, is probably due to the overlapping reduction of sulfate species and monomeric and/or polymeric VO_x species. With increasing calcination temperature, the left-hand shoulder nearly vanished and only one single reduction peak shifted to higher temperatures was observed for samples VTiS-723 (T_{m1} = 809 K) and VTiS-773 (T_{m1} = 820 K). At this high surface vanadium loading, the majority of the vanadia species were obviously present as crystalline V_2O_5 species, as confirmed by Raman spectroscopy. The monomeric and polymeric VO_x species are more easily reduced than crystalline V_2O_5 particles since the reduction peak maxima shifted to higher temperatures for crystalline V_2O_5 particles.

Furthermore, the H_2 consumption was found to be the highest for sample VTiS-673, suggesting stronger redox properties for this sample. This higher reducibility is possibly coming from a strong interaction with support. In addition, the lower H_2 consumption for samples VTiS-573 and VTiS-673 also indicated that the vanadium species were not fully oxidized at lower calcination temperatures. The percentage of V^{5+} species increased with increasing calcination temperatures.

3.4. Isopropanol probe reaction

The results of isopropanol (IPA) probe reaction over the samples in flowing air are presented in Table 5. The IPA probe reaction has been extensively used to characterize the surface acid/base proper-

Table 4
Reducibility of the catalysts as revealed by the H2-TPR measurements.

Catalyst	Surface V loading (V nm^{-2})[a]	T_{max}[b] (K)			H_2 consumption (mmol g^{-1})
			Peak 1 (T_{m1})	Peak 2 (T_{m2})	
VTiS-573	3.1	763	787	952	1.2
VTiS-623	3.5	777	798	953	1.7
VTiS-673	5.2	775	805	973	2.3
VTiSw50-673	5.3	754	786	965	2.2
VTiSw300-673	5.2	752	775	969	1.8
VTiS-723	15.1	760	809	n.d.[c]	2.1
VTiS-773	27.7	770	820	n.d.[c]	2.0

[a] Supposing that all vanadium atoms are located on the surface and calculated from Table 1.
[b] Maximum temperature of the TPR peaks.
[c] Not determined.

Table 5
Catalytic activities of VTiS catalysts in the isopropanol probe reaction at 393 K in air.

Sample	Conversion of IPA (%)	Selectivity (%)		
		PPE	ACE	DIPE
VTiS-573	3	16	65	19
VTiS-623	4	26	42	32
VTiS-673	7	22	51	27
VTiSw50-673	13	10	68	22
VTiSw300-673	11	6	80	14
VTiS-723	8	8	79	13
VTiS-773	3	11	77	12

IPA, isopropanol; PPE, propylene; DIPE, diisopropyl ether; ACE, acetone.

ties under N_2 flow [63] and probe the surface redox properties in an oxidative atmosphere [27]. Thus, the conversion of IPA and selectivity to propylene (PPE), diisopropyl ether (DIPE) and acetone (ACE) in air flow can be used to probe the strength of both surface acidic and redox properties.

Results in Table 5 showed that all the studied VTiS catalysts exhibited both surface acidic and redox properties since the dehydration products (PPE and DIPE) and oxidation product (ACE) formed. Sample VTiS-573 presented a low IPA conversion. Raising the calcination temperature increased the catalytic activity since the enhanced redox properties. For example, the conversion of IPA on VTiS-573 was only 3% while that on the VTiS-673 sample was 7%. The activity in the IPA conversion reaction reached a maximum value for the washed catalysts (VTiSw50-673 and VTiSw300-673), suggesting that the high content of sulfate poisoned the active species present on the surface. In addition, the conversion of IPA decreased when the calcination temperature increased from 723 K to 773 K, probably due to the a higher formation of less active crystalline V_2O_5 particles.

It can be seen from Table 5 that samples with high sulfur content seemed more acidic than oxidative since the dehydration products (PPE and DIPE) were enhanced, while the oxidation product ACE was inhibited. The comparison of acidity detected by IPA probe reaction and ammonia adsorption calorimetry was not completely consistent, probably because the IPA probe reaction provided relative information about acidic properties linked to redox properties while ammonia adsorption calorimetry measured absolute acidic properties independently of redox properties.

3.5. The selective oxidation of methanol to DMM

Catalysts consisting of pure vanadium pentoxide with coprecipitated titanium dioxide are recognized as suitable systems for partial oxidation of methanol [64,65]. Specially, sulfated vanadia–titania catalysts are starting to have new applications in the selective oxidation of methanol to dimethoxymethane (DMM) [10,25], which can undergo further steam reforming to produce hydrogen.

Table 6 presents the whole catalytic performances of VTiS and VTiSw catalysts calcined at different temperatures. In addition, Table 7 gives the turnover frequency (TOF) of catalysts, which is defined as the number of reactant molecules converted to products over one active catalyst site per second [66]. Fig. 14a and b show the effect of reaction temperature on methanol conversion and

Table 6
Catalytic activities of the VT and VTiS catalysts in the methanol oxidation reaction.

Sample	Temp. (K)	Conversion of methanol (%)	Selectivity (%)				
			DMM	FA	MF	DME	CO_x
VTiS-573	393	4	97	0	1	2	0
	403	6	96	0	2	2	0
	413	9	94	0	4	2	0
	423	12	89	3	5	2	0
	473	51	2	56	39	3	0
VTiS-623	393	4	98	0	0	2	0
	403	6	97	0	0	3	0
	413	10	96	0	1	3	0
	423	13	91	3	1	5	0
	473	63	1	61	27	11	0
VTiS-673	393	12	98	0	1	1	0
	403	18	98	0	1	1	0
	413	29	96	0	2	2	0
	423	43	92	1	5	2	0
	453	81	6	40	44	9	1
VTiSw50-673	393	47	95	1	4	0	0
	403	74	83	4	13	1	0
	413	87	38	19	42	1	0
	423	89	3	15	38	2	42
VTiSw300-673	393	41	91	3	5	1	0
	403	52	74	10	15	1	0
	413	82	5	12	83	5	0
	423	91	0	3	72	2	23
VTiS-723	393	10	98	0	1	1	0
	403	19	97	0	2	1	0
	413	30	95	0	4	1	0
	423	49	88	1	10	1	0
	443	92	1	2	79	2	16
VTiS-773	393	6	98	0	1	1	0
	403	10	98	0	1	1	0
	413	16	93	3	3	1	0
	423	19	80	12	7	1	0
	453	71	1	11	76	2	10

DMM: dimethoxymethane; FA: formaldehyde; MF: methyl formate; DME: dimethyl ether; CO_x: CO_2 (or CO).

Table 7
The turnover frequencies (TOFs) and characteristics of VTiS catalysts.[a]

Sample	N_s[b] (V nm^{-2})	Conversion of methanol (%) at 393 K	TOF[d] $\times 10^3$ (s^{-1})
VTiS-573	3.1	4	0.1
VTiS-623	3.5	4	0.1
VTiS-673	5.2	12	0.4
VTiSw50-673	5.3	47	1.4
VTiSw300-673	5.2	41	1.2
VTiS-723	7.9[c]	10	0.6
VTiS-773	7.9[c]	6	0.6

[a] Feed conditions: methanol:O_2:N_2 = 2:6:30 mL min^{-1}, catalyst loading 0.2 g.
[b] N_s is the number of exposed catalytic active vanadium atoms per square meter.
[c] The theoretical number of exposed vanadium atoms per square meter on TiO_2 for the monolayer coverage.
[d] TOF of methanol conversion at 393 K.

DMM selectivity for all the catalysts. As presented in Table 6 and Fig. 14a and b, high reaction temperature adversely affects selectivity to DMM while it enhances the methanol conversion and selectivity to formic acid (FA) and carbon oxides. DMM remained the predominant product in the temperature range used (393–423 K). Beyond this value ($T_{react} \geqslant 425$ K), a sudden drop in the DMM selectivity was observed for all the studied catalysts. This behavior is possibly as a result of thermodynamic constraints for DMM synthesis [11]. As shown in Fig. 14a, the tendency of catalytic activity of VTiS catalysts for methanol oxidation reaction is in consistence with the order obtained from isopropanol conversion. Moreover, it was confirmed that enhanced redox properties increased catalytic activity. Among all the VTiS catalysts, the best catalytic performances were observed for samples VTiS-673 (423 K: $Con_{methanol}$ = 43%; S_{DMM} = 92%) and VTiS-723 (423 K: $Con_{methanol}$ = 49%; S_{DMM} = 88%), which displayed completely different structures of surface vanadium oxide phase. Amorphous polymeric VO_x species with terminal V=O bonds were observed only on sample VTiS-673, as indicated by Raman spectroscopy and TPR experiments, while separated phases of crystalline vanadia and titania were revealed by SEM and TEM experiments for sample VTiS-723. As reported in literature [13–15,17,18], surface structures constituted by terminal V=O are more active for DMM formation compared to crystalline V_2O_5. Further, the amorphous character of catalyst is also an important parameter since the methanol conversion to DMM requires the cooperative work of two types of sites (acid and redox) [67]. Accordingly, sample VTiS-673 should present better catalytic ability than VTiS-723.

Nevertheless, the difference between samples VTiS-673 and VTiS-723 resides not only in the surface structure but also in the sulfur concentration as presented in Table 1 (VTiS-673: *S*% = 2.6%; VTiS-723: *S*% = 0.7%). Thus, the effects of sulfur content on catalytic performance were investigated by the comparison of reactivity between VTiS-673 and VTiSw-673 catalysts, as shown in Fig. 14b. With decreasing sulfur content, obtained by washing with water, an increase in methanol conversion and a decrease in DMM selectivity were simultaneously observed. An excellent catalytic behavior with high DMM yield at the very low reaction temperature of 403 K was obtained for sample VTiSw50-673 (methanol conversion = 74%; S_{DMM} = 83%), which contained a proper amount of sulfur (*S* = 0.8%). The data show that the catalytic activity can be deeply influenced by the VO_x species nature and sulfur content. Moreover, the TOFs calculated from the number of exposed active vanadium sites for each catalyst can help in providing the intrinsic activity of the catalysts. The number of exposed surface vanadium active sites was referenced to the N_s (surface vanadium sites per square meter) value of the theoretical vanadia monolayer surface (7.9 V nm^{-2}) [66]. Below monolayer coverage, N_s was simply taken as the number of surface vanadium atoms in the catalysts (shown in Table 4, column 1). Above monolayer coverage, the N_s was taken as the theoretical value of 7.9 V nm^{-2}. As shown in Table 7, similar TOFs of the surface vanadium sites in the sub-monolayer region were obtained for VTiS-573, -623, and -673 catalysts containing increasing vanadium contents and similar sulfur contents. This is in agreement with previous observations [68,69] that the methanol oxidation activity is independent of the concentration of vanadium sites below the monolayer coverage. Deo and Wachs [69] also concluded that this selective oxidation reaction involves only one surface VO_4 site. Oppositely, TOF values vary by one order of magnitude from 4×10^{-4} s^{-1} (VTiS-673) to $\sim 1.2 \times 10^{-3}$ s^{-1} (VTiSw-673) for both samples calcined at 673 K but with different amounts of sulfur, thus revealing that sulfur would poison surface

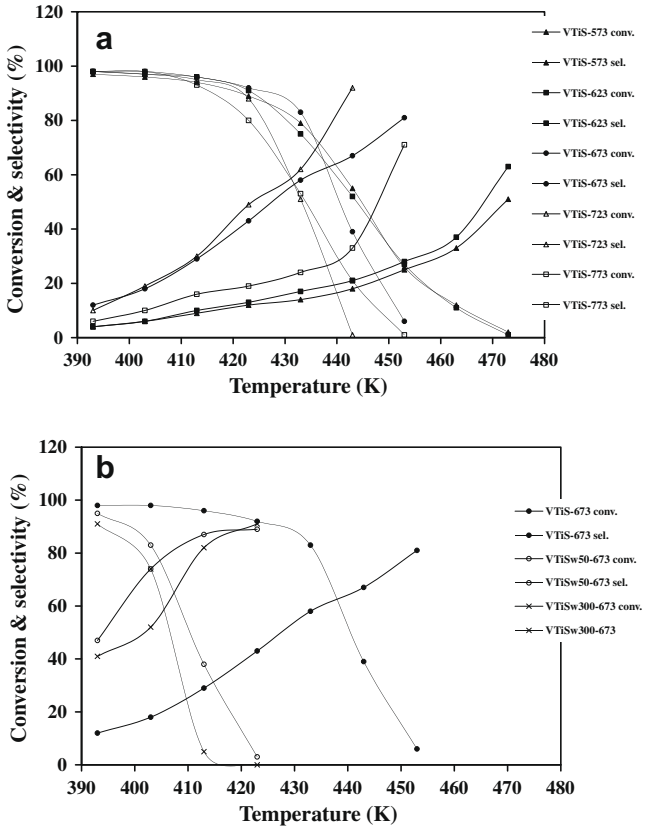

Fig. 14. DMM selectivity and methanol conversion vs. reaction temperatures over: (a) VTiS catalysts and (b) VTiSw catalysts.

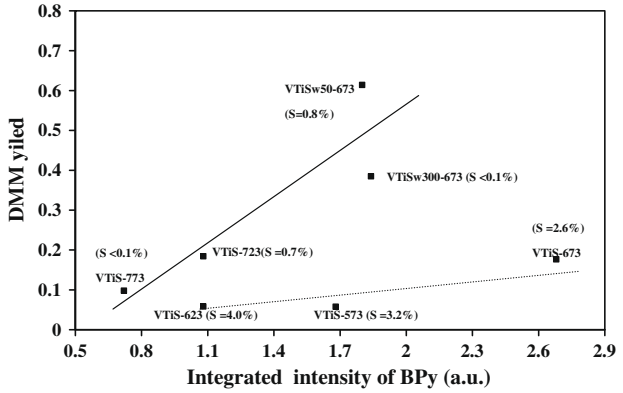

Fig. 15. Correlation between the integrated intensity relative to Brönsted acid sites (FTIR) and DMM yield.

active vanadium sites and thus decrease the catalytic activity. For samples VTiS-723 and VTiS-773 above monolayer coverage (>7.9 V nm^{-2}), the surface vanadium atoms correspond to a mixture of surface VO_4 sites and crystalline V_2O_5 sites. Thus, the relatively decreased TOF values, compared with VTiSw-673 samples, suggest that crystalline V_2O_5 phase did not contribute to the catalytic activity.

In addition, according to the above investigation by pyridine adsorption FTIR, the relative concentrations of Brönsted and Lewis acid sites were influenced by the sulfur content. In particular, the Brönsted acidity at 403 K was compared with the DMM yield at the same reaction temperature. Fig. 15 shows interesting correlations between the relative concentration of Brönsted acid sites and the DMM yield. For the VTiSw50-673, VTiSw300-673, VTiS-723, and VTiS-773 samples containing low sulfur content, the DMM yield increased quasi linearly with increasing concentration of Brönsted acid sites, suggesting that Brönsted acid sites promoted the catalytic activity. However, for VTiS-573, VTiS-623, and VTiS-673 samples with high content of sulfur, although possessing an appreciable number of Brönsted acid sites, the DMM yield did not increase remarkably with increasing concentration of Brönsted acid sites. This suggests that the high content of sulfur increased the number of Brönsted acid sites but poisoned the catalyst, which is consistent with the TOF values shown in Table 7. No evident correlation was found between the concentration of Lewis acid sites of catalysts and the DMM yield. The relationship proposed here offers a reasonable explanation of the catalytic performances shown in Table 6 and Fig. 14.

Therefore, the Brönsted acid sites and amorphous polymeric VO_x species with terminal V=O bonds of the samples possessing low sulfur content as well as redox properties are confirmed to be responsible for optimal DMM synthesis.

4. Conclusion

In the present study, sulfated vanadia–titania catalysts (S_{BET}: 57–402 $m^2\ g^{-1}$) containing different amounts of sulfur (0.1–4.0 wt.%) were prepared by co-precipitation. The influence of calcination temperature and washing with water, which determine the nature of VO_x species (polymeric and crystalline) and acidic sites, on the partial oxidation of methanol to DMM was investigated. The Raman spectra and TPR profiles of the VTiS and VTiSw catalysts provided complementary information about the nature of the vanadia species: (1) highly amorphous VO_x species were formed at the calcination temperatures of 573 and 623 K, (2) terminal V=O bonds and V–O–V linkages were obtained for samples calcined at 673 K, and (3) crystalline V_2O_5 species were observed when the calcination temperature was higher than 723 K. Additionally, as shown by SEM and TEM images, needle-like crystalline V_2O_5 species grew away from the TiO_2 surface, suggesting separated phases of V_2O_5 and TiO_2. The skeletal FTIR spectra of VTiS catalysts before and after catalytic test of methanol conversion revealed that appropriate surface hydroxyl groups and sulfate species could be the active sites in catalysts. The ammonia adsorption calorimetry study showed that the number of medium strength acid sites with $90 < Q_{diff} < 120$ kJ mol^{-1}, considered to be the active Brönsted acid sites as confirmed by pyridine FTIR measurements, is highest for sample VTiS-673. The comparison of Brönsted and Lewis acidities between VTiS-673 and VTiSw-673 samples, performed by pyridine adsorption FTIR, indicated a transformation reaction of Brönsted acid sites to Lewis acid sites after removal of some sulfate species from the surface by washing the sample with deionized water. In addition, a high concentration of sulfur can favor the formation of weak Brönsted acid sites and to some extent inhibit the creation of strong acid sites. The comparison of TOF values between washed (VTiSw-673) and unwashed (VTiS-673) samples for oxidation of methanol revealed that a high content of sulfate species would poison catalytically active sites, as confirmed by the isopropanol probe reaction. The best catalytic performance was observed for sample VTiSw50-673 with the highest DMM yield (methanol conversion:74%; S_{DMM}:83%) at the very low reaction temperature of 403 K. Consequently, an appropriate calcination temperature of 673 K with proper concentration of sulfur (~0.8 wt.%) generated polymeric VO_x species with terminal V=O bonds, high Brönsted acidity, and enhanced reducibility. These are critical parameters for optimizing DMM production.

Acknowledgments

The authors are thankful to the scientific services of Ircelyon, particularly to Mimoun Aouine and Laurence Burel for providing SEM and TEM measurements.

Hongying Zhao gratefully acknowledges the China Scholarship Council for the financial support of her PhD grant.

Financial supports from NSFC (20673055) and MSTC (2005CB221400 and 2004DFB02900) are acknowledged.

References

[1] K. Fuji, S. Nakano, E. Fujita, Synthesis 4 (1975) 276–277.
[2] Q. Sun, A. Auroux, J. Shen, J. Catal. 244 (2006) 1–9.
[3] H. Friedrich, W. Neugebauer, US Patent 3 843 562 (1974).
[4] S. Satoh, Y. Tanigawa, US Patent 6 379 507 (2002).
[5] Y. Yuan, H. Liu, H. Imoto, T. Shido, Y. Iwasawa, J. Catal. 195 (2000) 51–61.
[6] Y. Yuan, Y. Iwasawa, J. Phys. Chem. B 106 (2002) 4441–4449.
[7] H. Liu, N. Bayat, E. Iglesia, Angew. Chem. Int. Ed. 42 (2003) 5072–5075.
[8] H. Liu, E. Iglesia, J. Phys. Chem. B 109 (2005) 2155–2163.
[9] Y. Zhang, I.J. Drake, D.N. Briggs, A.T. Bell, J. Catal. 244 (2006) 219–229.
[10] Y. Fu, J. Shen, Chem. Commun. 21 (2007) 2172–2174.
[11] H. Liu, E. Iglesia, J. Catal. 223 (2004) 161–169.
[12] I.E. Wachs, T. Kim, in: D. Jackson, J. Hargreaves (Eds.), Metal Oxide Catalysis, vol. 2, Wiley-VCH, 2009, pp. 487–497.
[13] G.C. Bond, J. Chem. Technol. Biotechnol. 68 (1997) 6–13.
[14] C.R. Dias, M.F. Portela, G.C. Bond, J. Catal. 157 (1995) 344–352.
[15] G. Centi, Appl. Catal. A: Gen. 147 (1996) 267–298.
[16] B. Grzybowska-Swierkosz, Appl. Catal. A: Gen. 157 (1997) 263–310.
[17] J.M. Tatibouët, Appl. Catal. A: Gen. 148 (1997) 213–252.
[18] J.M. Tatibouët, J.E. Germain, J. Catal. 72 (1981) 375–378.
[19] A. Gervasini, P. Carniti, J. Keränen, L. Niinistö, A. Auroux, Catal. Today 96 (2004) 187–194.
[20] A.J. Van Hengstum, J.G. Van Ommen, H. Bosch, P.J. Gellings, Appl. Catal. 8 (1983) 369–382.
[21] B.M. Weckhuysen, D.E. Keller, Catal. Today 78 (2003) 25–46.
[22] M. Calatayud, C. Minot, Top. Catal. 40 (2006) 17–26.
[23] I.E. Wachs, B.M. Weckhuysen, Appl. Catal. A: Gen. 157 (1997) 67–90.
[24] D.A. Bulushev, F. Rainone, L. Kiwi-Minsker, Catal. Today 96 (2004) 195–203.
[25] H. Zhao, S. Bennici, J. Shen, A. Auroux, J. Mol. Catal. A: Chem. 309 (2009) 28–34.
[26] H. Zhao, S. Bennici, J. Cai, J. Shen, A. Auroux, Catal. Today, (2009), in press, doi:10.1016/j.cattod.2009.08.005.
[27] H. Zhao, S. Bennici, J. Shen, A. Auroux, Appl. Catal. A: Gen. 356 (2009) 121–128.
[28] P. Malet, A. Caballero, J. Chem. Soc., Faraday Trans. I 84 (1988) 2369–2375.
[29] D.A.M. Monti, A. Baiker, J. Catal. 83 (1983) 323–335.
[30] S.L.T. Andersson, J. Chem. Soc., Faraday Trans. I 75 (1979) 1356–1370.
[31] J.A. Odriozola, J. Soria, G.A. Somorjai, H. Heinemann, J.F. Garcia de la Banda, M. Lopez Granados, J.C. Conesa, J. Phys. Chem. 95 (1991) 240–246.
[32] M.H. Kim, I.S. Nam, Y.G. Kim, J. Catal. 179 (1998) 350–360.
[33] J.P. Chen, R.T. Yang, J. Catal. 139 (1993) 277–288.
[34] F.D. Hardcastle, I.E. Wachs, J. Phys. Chem. 95 (1991) 5031–5041.
[35] J. Twu, P.K. Dutta, J. Phys. Chem. 93 (1989) 7863–7868.
[36] J. Twu, P.K. Dutta, J. Catal. 124 (1990) 503–510.
[37] J.P. Dunn, J.M. Jehng, D.S. Kim, L.E. Briand, H.G. Stenger, I.E. Wachs, J. Phys. Chem. B 102 (1998) 6212–6218.
[38] N. Kausar, R. Howe, M. Skyllas-Kazacos, J. Appl. Electrochem. 31 (2001) 1327–1332.
[39] I. Giakoumelou, R.M. Caraba, V.I. Parvulescu, S. Boghosian, Catal. Lett. 78 (2002) 209–214.
[40] I.R. Beattie, T.R. Gilson, J. Chem. Soc. A (1969) 2322–2327.
[41] F. Roozeboom, M.C. Mittelmeijer-Hazeleger, J.A. Moulljn, J. Medema, V.H.J. De Beer, P.J. Gellings, J. Phys. Chem. 84 (1980) 2783–2791.
[42] I.E. Wachs, Catal. Today 27 (1996) 437–455.
[43] G. Socrates, Infrared Characteristic Group Frequencies, second ed., pp. 168–169.
[44] O. Saur, M. Bensitel, A.B. Mohammed Saad, J.C. Lavalley, C.P. Tripp, B.A. Marrow, J. Catal. 99 (1986) 104–110.

[45] M.A. Fox, M.T. Dulay, Chem. Rev. 93 (1993) 341–357.
[46] L. Nalbandian, A.A. Lemonidou, Thermochim. Acta 419 (2004) 149–159.
[47] A. Auroux, Top. Catal. 4 (1997) 71–89.
[48] A. Desmartin-Chomel, J.L. Flores, A. Bourane, J. M Clacens, F. Figueras, G. Delahay, A. Giroir-Fendler, C. Lehaut-Burnouf, J. Phys. Chem. B 110 (2006) 858–863.
[49] A. Gervasini, J. Fenyvesi, A. Auroux, Langmuir 12 (1996) 5356–5364.
[50] S. Bennici, A. Auroux, in: D. Jackson, J. Hargreaves (Eds.), Metal Oxide Catalysis, vol. 1, Wiley-VCH, 2009, pp. 391–436.
[51] H. Miyata, Y. Nakagawa, S. Miyagawa, Y. Kubokawa, J. Chem. Soc., Faraday Trans. 1 (84) (1988) 2129–2134.
[52] J. Datka, A.M. Turek, J.M. Jehng, I.E. Wachs, J. Catal. 135 (1992) 186–199.
[53] J. Keränen, A. Auroux, L. Niinistö, Appl. Catal. A 228 (2002) 213–225.
[54] H. Miyata, K. Fujii, S. Inui, Y. Kubokawa, Appl. Spectrosc. 40 (1986) 1177–1180.
[55] G. Connell, J.A. Dumesic, J. Catal. 105 (1987) 285–298.
[56] E. Ortiz-Islas, T. Lopez, J. Navarrete, X. Bokhimi, R. Gomez, J. Mol. Catal. A: Chem. 228 (2005) 345–350.
[57] T. Barzetti, E. Selli, D. Moscotti, L. Forni, J. Chem. Soc., Faraday Trans. 92 (1996) 1401–1407.
[58] B.Q. Xu, W.M.H. Sachtler, J. Catal. 167 (1997) 224–233.
[59] G.C. Bond, S.F. Tahir, Appl. Catal. 71 (1991) 1–31.
[60] G.Y. Popova, T.V. Andrushkevich, E.V. Semionova, Y.A. Chesalov, L.S. Dovlitova, V.A. Rogov, V.N. Parmon, J. Mol. Catal. A: Chem. 283 (2008) 146–152.
[61] D.A. Bulushev, L. Kiwi-Minsker, F. Rainone, A. Renken, J. Catal. 205 (2002) 115–122.
[62] G. Deo, I.E. Wachs, J. Haber, Crit. Rev. Surf. Chem. 4 (1994) 141–187.
[63] A. Gervasini, J. Fenyvesi, A. Auroux, Catal. Lett. 43 (1997) 219–228.
[64] F. Roozeboom, P.D. Cordingley, P.J. Gellings, J. Catal. 68 (1981) 464–472.
[65] A. Baiker, D. Monti, J. Catal. 91 (1985) 361–365.
[66] T. Kim, I.E. Wachs, J. Catal. 255 (2008) 197–205.
[67] S. Royer, X. Sécordel, M. Brandhorst, F. Dumeignil, S. Cristol, C. Dujardin, M. Capron, E. Payen, J.L. Dubois, Chem. Commun. 7 (2008) 865–867.
[68] C.M. Sorensen, R.S. Weber, J. Catal. 142 (1993) 1–17.
[69] G. Deo, I.E. Wachs, J. Catal. 146 (1994) 323–334.